Optical tweezers for undergraduates: Theoretical analysis and experiments

M. S. Rocha[a)]
Departamento de Física, Universidade Federal de Viçosa, CEP 36570-000 Viçosa, Minas Gerais, Brazil

(Received 30 December 2008; accepted 28 April 2009)

A theoretical treatment of optical tweezers is presented at a level suitable for undergraduates. We explore the Rayleigh and the geometrical optics regimes with an emphasis on the latter. We discuss a model for the geometrical optics regime, including spherical aberration effects, and show that the model can easily be implemented numerically. A comparison of the model with experimental data yields excellent agreement between theory and experiment. We also briefly discuss a theory of optical tweezers valid for microspheres of any size. © *2009 American Association of Physics Teachers.*
[DOI: 10.1119/1.3138698]

I. INTRODUCTION

A single laser beam focused by a high numerical aperture microscope objective is able to trap dielectric particles (usually microspheres) near the lens focus. Such an arrangement is called optical tweezers[1–3] and has a wide range of applications in physics and biology.[4–16] Optical tweezers have been used to manipulate and study objects such as microspheres, macromolecules such as DNA and RNA, and even live cells. A particular characteristic of the technique is the possibility to trap individual objects, which can then be studied alone, free from the influence of other objects in the sample. Some helpful reviews of optical tweezers have been published recently.[6,17,18]

In this paper, we present a theoretical treatment of optical tweezers at a level suitable for undergraduate students. In Sec. II we discuss the phenomenon qualitatively and show how a single laser beam can trap a dielectric microsphere. Next we explore the Rayleigh and the geometrical optics regimes. The Rayleigh regime is usually valid for beads for which the radius a is much smaller than the laser wavelength λ.[19,20] This regime is discussed in detail in Sec. III. The geometrical optics regime is usually valid for beads for which the radius a is much larger than the laser wavelength.[2,21] We discuss this regime in detail in Sec. IV and present a theoretical model that includes spherical aberration effects.

Spherical aberration is present in most experimental situations. To understand this phenomenon, consider Fig. 1(a). This figure represents a laser beam focused by an oil immersion microscope objective, reaching an imaginary bead (this setup is frequently used for optical tweezers). This figure is extremely simplified because we are not considering the beam refraction at the sample interfaces; a more realistic representation is shown in Fig. 1(b). The laser beam is refracted when it passes from the glass coverslip to the medium (generally water) in which the beads are located at the sample chamber. It is not necessary to consider refraction at the other interfaces because the oil refractive index matches very closely the glass refractive index.[22,23] In other words, spherical aberration arises from the refractive index mismatch at the glass-water interface of the sample. Observe that in Fig. 1(a) the laser focus without aberration is a single point. Nevertheless, the real situation is represented in Fig. 1(b). In fact, spherical aberration degrades the laser focus and decreases the trapping efficiency. Therefore, it is important to include this effect in any theory of optical tweezers.[19,23–28]

A bead trapped by optical tweezers behaves like a harmonic oscillator. When the bead is displaced from its equilibrium position in the potential well of the tweezers for small displacements, it experiences a restoring force proportional to the displacement. In addition, the trapped bead executes Brownian motion while trapped in the potential well. For this reason, this system is sometimes called a Brownian harmonic oscillator.

In this paper, we calculate the force and the trap stiffness for optical tweezers in the geometrical optics regime, taking spherical aberration into account. The results are compared with experimental data in this regime.[22,23] Geometrical optics is very useful pedagogically when analyzing optical tweezers. In addition, geometrical optics results serve as a guide for the introduction of spherical aberration in more realistic theories.[22,23] To evaluate the force exerted by a laser beam on a microsphere, we first calculate it for a "single ray" (we employ this abbreviation for a thin pencil of rays) and then we sum (integrate) over all rays from the beam, as we discuss in Sec. IV.

The force exerted by a strongly focused laser beam on a dielectric microsphere with arbitrary radius and refractive index was recently derived by Maia Neto and co-workers[22,23,29,30] within the framework of the Mie–Debye spherical aberration theory. This theory is the most complete and realistic theory of optical tweezers and is discuss in Sec. VII. An important feature of this theory is that it involves no adjustable parameters, that is, all parameters used to calculate the trap stiffness can be measured, so we can perform an absolute comparison between theory and experiments.[22,23]

II. PRELIMINARY ANALYSIS

The development of electromagnetic theory by Maxwell and others showed that light can transfer momentum to objects. The resultant force depends on the velocity v in the medium in which the light travels. For a single ray with power P_r, we can write

$$F \propto \frac{P_r}{v} \tag{1}$$

with

$$v = \frac{c}{n_m}, \tag{2}$$

where n_m is the refractive index of the medium and c is the light velocity in vacuum.

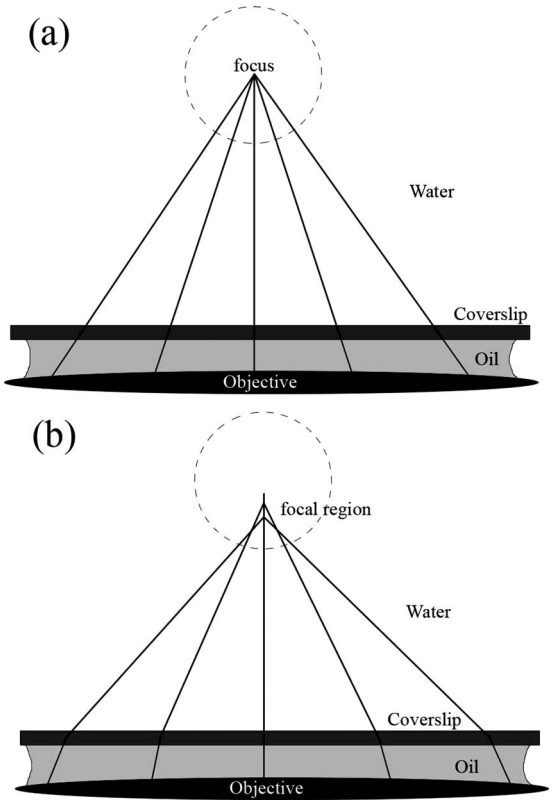

Fig. 1. Spherical aberration in optical tweezers. (a) Idealized situation without spherical aberration. (b) Real situation in most experimental setups. The focus is degraded due to the laser refraction at the glass-water interface of the sample, decreasing the trapping efficiency.

To estimate the magnitude of the force exerted by light, consider a light beam incident perpendicularly on a plane mirror. Each photon has a momentum $\hbar\vec{k}$, where $\vec{k}$ is the light wave vector. When reflected, this photon acquires a momentum $-\hbar\vec{k}$, and the momentum transferred to the mirror is $\Delta\vec{p}=2\hbar\vec{k}$. Its magnitude can be written as

$$\Delta p = 2\hbar k = 2\frac{\hbar\omega}{v} = 2\frac{E}{v}, \tag{3}$$

where E is the photon energy and ω is the angular frequency.

The force exerted by a beam with N photons per second incident on the mirror can then be written using Newton's second law as

$$F = 2\frac{1}{v}\frac{dE_{\text{beam}}}{dt} = 2\frac{P_{\text{beam}}}{v}. \tag{4}$$

For optical tweezers, the typical power used is of the order of a few milliwatts, and Eq. (4) predicts a force of the order of piconewtons ($1\ \text{pN}=10^{-12}$ N). A force with this magnitude is extremely small and can be measured more easily using objects with sizes at the micrometer range (or smaller).

This analysis is related to the reflection of the beam at the object's surface. The force that results from this effect is known as radiation pressure. This force cannot explain optical trapping because its effect is to push the object in the direction of the incident beam. To understand how a laser beam can trap an object, we must consider gradient forces, which are present when the beam is focused to a certain point.

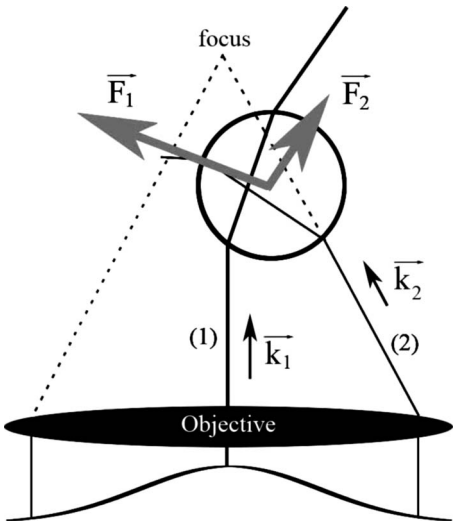

Fig. 2. Two rays (wave vectors k_1 and k_2) from the beam are represented, refracting at a bead localized below the focus. The rays exert forces F_1 and F_2 when refracted on the bead surface. The resulting gradient force points to the laser focus.

Gradient forces are related to the beam refraction at the object's surface. Because the wave vector $\vec{k}$ of each ray is changed during refraction, its momentum is also changed. Therefore, the object also experiences a momentum change (in the opposite direction) due to momentum conservation of the combined system (beam plus object). This fact implies that a force acts on the object to change its momentum. Figure 2 depicts this situation and represents two rays from the beam, refracting at the microsphere's surface. Ray 1, with wave vector k_1, comes from the central portion of the beam, which is represented by a Gaussian intensity profile before the objective (this kind of profile is the standard one used in optical tweezers). This ray generates a force F_1 on the microsphere when refracted. Ray 2, with wave vector k_2, comes from the right hand portion of the beam profile and generates a force F_2 on the microsphere. Note that $|F_1|>|F_2|$ because the intensity profile has a Gaussian shape. Therefore, the resulting force points toward the laser focus. These two rays were used to represent the global effect of all rays from the beam, coming from the central portion and from the right hand portion of the intensity profile. Figure 3 depicts another situation in which the bead is above the objective focus. Observe that the resulting force also points toward the focus in this situation. It is easy to see that the resulting force always points toward the focus for any position of the microsphere relative to the focus. This qualitative analysis explains optical trapping.

In real situations we usually have both gradient forces and radiation pressure because the rays are partially refracted and partially reflected at the microsphere's surface. The microsphere remains trapped when the gradient force is the dominant one, which occurs when the beam is highly focused by the microscope objective. The analysis depicted in Figs. 2 and 3 was performed in the geometrical optics regime. This regime will be discussed in Sec. IV.

III. RAYLEIGH REGIME

The treatment presented in this section is usually appropriate for small beads. The Rayleigh regime is valid when the beam phase shift is small when refracted at the bead, or

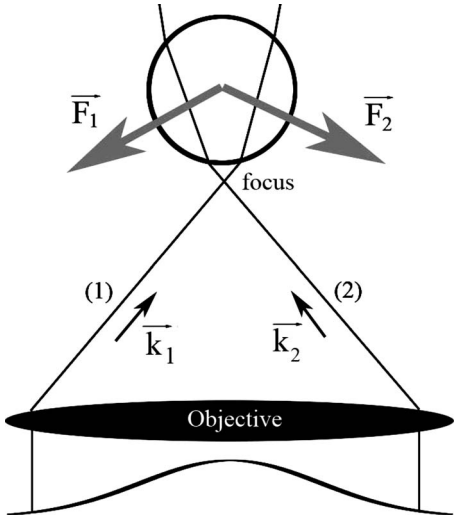

Fig. 3. Two rays (wave vectors k_1 and k_2) from the beam are represented, refracting at a bead localized above the focus. The rays exert forces F_1 and F_2 when refracted on the bead surface. The resulting gradient force also points to the laser focus in this case.

$$2ka(\mu-1) \ll 1, \tag{5}$$

where k is the wave vector in the medium surrounding the bead, a is the bead radius, and μ is the relative refractive index, $\mu=n_s/n_m$ (n_s and n_m are the refractive indices of the sphere and medium, respectively).

In many experimental setups infrared lasers are used for optical tweezers. Also, the medium surrounding the beads is usually water, and the condition $\mu>1$ is usually valid. Therefore, the condition in Eq. (5) can be simplified in most cases to $a \ll \lambda$ (remember that $k=2\pi n_m/\lambda$). In this regime we cannot use a geometrical optics analysis, as illustrated in Figs. 2 and 3.

Because the bead is very small, it can be considered to be an induced dipole in an approximately uniform electric field due to the laser.[20,29,30] The problem of a dielectric sphere located in a uniform electric field is solved in many books on electromagnetic theory.[31] The induced dipole moment of the dielectric sphere can be written as

$$\vec{p} = \frac{K-1}{K+2} a^3 \vec{E}, \tag{6}$$

where $\vec{E}$ is the electric field outside the microsphere and K is defined as

$$K = \frac{\epsilon}{\epsilon_m}, \tag{7}$$

where ϵ and ϵ_m are the electric permittivities of the microsphere and of the medium, respectively.

The electric potential energy of the induced dipole can then be written as

$$U = -\vec{p}\cdot\vec{E}, \tag{8}$$

and the force on the bead is

$$\vec{F} = -\vec{\nabla}U = \vec{\nabla}(\vec{p}\cdot\vec{E}). \tag{9}$$

By using Eqs. (6) and (9), we can write

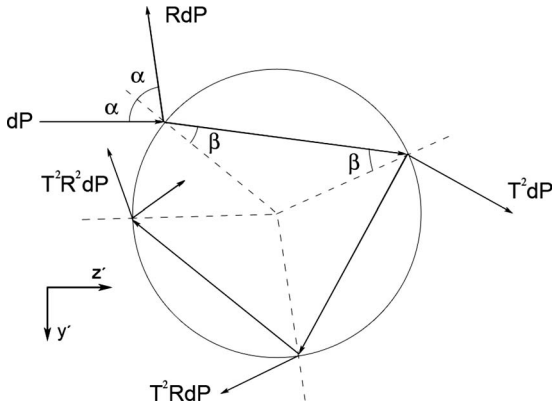

Fig. 4. An incident ray undergoing multiple internal reflections and refractions on a bead.

$$\vec{F} = \frac{K-1}{K+2} a^3 \vec{\nabla} E^2. \tag{10}$$

Note that this force is proportional to the gradient of the field intensity, which means that the force points toward the field region with maximum intensity, that is, the focus. This simple analysis explains why the beads stay trapped in the focal region of a convergent beam in the Rayleigh regime.

To conclude this analysis, we calculate the trap stiffness of the optical tweezers. The x-component of the force is

$$F_x = \frac{K-1}{K+2} a^3 \frac{\partial E^2}{\partial x}, \tag{11}$$

and the trap stiffness is defined as

$$\kappa_x = -\left(\frac{\partial F_x}{\partial x}\right)_{\vec{r}_{eq}} = -\frac{K-1}{K+2} a^3 \left(\frac{\partial^2 E^2}{\partial x^2}\right)_{\vec{r}_{eq}}, \tag{12}$$

where $\vec{r}_{eq}$ is the equilibrium position of the microsphere. We conclude that, in the Rayleigh regime, the trap stiffness is proportional to a^3.

IV. GEOMETRICAL OPTICS REGIME

The treatment in this section is usually appropriate for large beads, that is,

$$2ka(\mu-1) \gg 1. \tag{13}$$

For typical experimental situations, this condition can be simplified to $a \gg \lambda$, as discussed in Sec. III. In this situation, a treatment based on geometrical optics is valid.

We now calculate the force exerted by the laser beam on the bead in the geometrical optics regime. We first calculate the force exerted by a single ray on the bead and then integrate this result for the entire beam to obtain the force exerted by the optical tweezers on the bead. We include spherical aberration effects in this treatment, which are present in most experimental situations.

A. Force exerted by a single ray

Figure 4 shows a single ray with power dP incident on a microsphere in the direction $\hat{z}'$. We also show some multiple reflected and refracted rays generated by the incident ray. We denote by R and T the reflectivity and transmissivity at the medium-sphere interface, respectively, and by α and β the

angles of incidence and refraction. Each ray in Fig. 4 is labeled with the corresponding power, determined by the number of reflections and refractions that it undergoes.

The resulting force exerted by the single ray on the bead was first calculated by Roosen[21] and Ashkin.[2] They obtained this force by summing the infinite series of multiple reflections and refractions, which can then be used to determine the variation in the bead momentum. Therefore, the force can be calculated by applying Newton's second law. The result can be written as[21,2]

$$d\vec{F} = \frac{n_m}{c}[\mathrm{Re}(Q_t)\hat{z}' + \mathrm{Im}(Q_t)\hat{y}']dP, \tag{14}$$

where $\hat{z}'$ and $\hat{y}'$ are the unit vectors indicated in Fig. 4, and

$$Q_t = 1 + R\exp(2i\alpha) - T^2\frac{\exp[2i(\alpha-\beta)]}{1 + R\exp(-2i\beta)}. \tag{15}$$

The expressions for the reflectivity R and transmissivity T can be written by taking an average over the two laser polarizations, TE and TM (Ref. 31) (assuming no preferential polarization),

$$R(\alpha,\beta) = \frac{1}{2}\left[\frac{\sin(\alpha-\beta)}{\sin(\alpha+\beta)}\right]^2 + \frac{1}{2}\left[\frac{\tan(\alpha-\beta)}{\tan(\alpha+\beta)}\right]^2 \tag{16}$$

and

$$T(\alpha,\beta) = 1 - R(\alpha,\beta). \tag{17}$$

The total force exerted by the optical tweezers is obtained by integrating Eq. (14) over all rays from the incident laser beam. To do so and to make quantitative comparisons between theoretical and experimental results, we need to know the intensity profile of the laser beam.

B. Intensity profile at the entrance of the objective

The intensity profile at the objective entrance displays the usual Gaussian shape in most experimental setups. This profile must be measured to determine the beam waist σ. Viana *et al.*[22,23] employed two techniques to measure the beam waist. The first technique consists of analyzing a digital image of the laser beam with a ruler calibration; the second technique consists of measuring the intensity profile from the laser power going through a diaphragm as a function of its radius.

The measured intensity profile can be fitted to the expression

$$I(\rho) = I_0\exp\left(\frac{-\rho^2}{2\sigma^2}\right), \tag{18}$$

which determines the beam waist σ.

C. Reference frame

We take the origin of the reference frame at the objective focus, as indicated in Fig. 5. We label a particular incident ray by its coordinate ρ before it passes through the objective. After the objective it is more convenient to label the ray by the angle θ. Given the intensity profile at the objective entrance, the power element dP in Eq. (14) can be calculated using $dP = I(\rho)dA$, where dA is an area element of the objective and $I(\rho)$ is given by Eq. (18). In cylindrical coordinates, we write

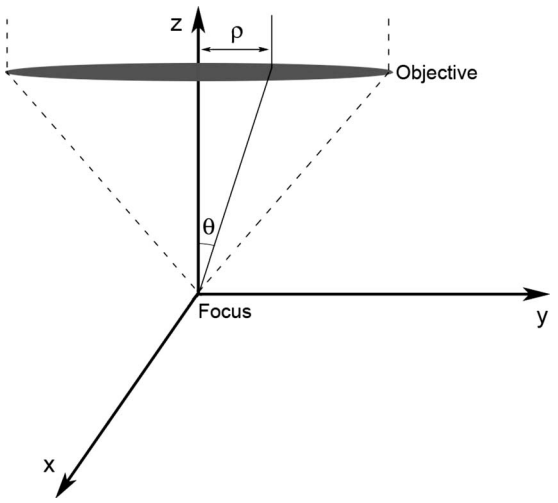

Fig. 5. Coordinate reference frame employed in the calculations.

$$dP = I_0\exp\left(\frac{-\rho^2}{2\sigma^2}\right)\rho d\rho d\varphi, \tag{19}$$

where φ is the azimuthal angle. Equation (19) can be written in terms of the total beam power before the coverslip,

$$dP = \frac{P_t}{2\pi\sigma^2}\exp\left(\frac{-\rho^2}{2\sigma^2}\right)\rho d\rho d\varphi \tag{20}$$

with

$$P_t = \int_0^{2\pi}\int_0^{\infty} I_0\exp\left(\frac{-\rho^2}{2\sigma^2}\right)\rho d\rho d\varphi. \tag{21}$$

We use the Abbe sine condition, which is essential to have a proper description of microscope objectives,[29,30]

$$\rho = f\sin\theta, \tag{22}$$

where f is the focal length of the objective, which can be written as

$$f = \frac{n_g R}{\mathrm{NA}}, \tag{23}$$

in which n_g is the glass refractive index (objective), R is the maximum value of ρ, and NA is the numerical aperture of the objective.

We substitute Eq. (22) into Eq. (20) and obtain the power element,

$$dP = \frac{P_t}{2\pi\sigma^2}\exp\left(\frac{-f^2\sin^2\theta}{2\sigma^2}\right)f^2\sin\theta\cos\theta d\theta d\varphi. \tag{24}$$

Some rays from the beam do not reach the bead because they undergo total internal reflection at the glass-medium interface. Therefore, it is more convenient to rewrite Eq. (24) in terms of the local power P_l reaching the bead. We can determine this local power by excluding the rays that are blocked at the entrance of objective, as well as those undergoing total internal reflection at the glass-medium interface. P_l can be written as a function of P_t as[29]

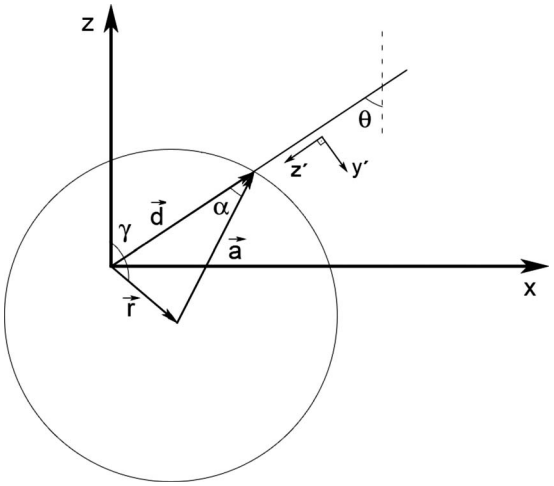

Fig. 6. Change in variables in the aberration-free case.

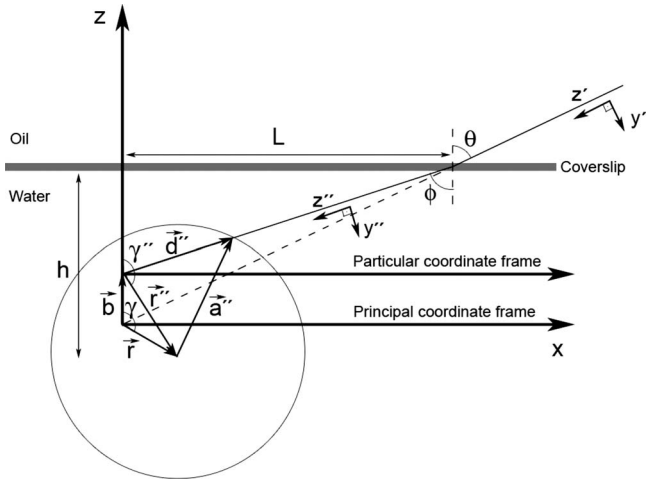

Fig. 7. Change in variables in the general situation, including spherical aberration.

$$P_l = \int_0^{2\pi}\int_0^{\theta_0} dP = P_t\left[1-\exp\left(\frac{-f^2\sin^2\theta_0}{2\sigma^2}\right)\right], \tag{25}$$

where θ_0 is the maximum value of θ corresponding to the ray that reaches the bead with the maximum deviation from the incident direction of the beam.

We then write dP as a function of P_l,

$$dP = \frac{P_l \exp\left(\frac{-f^2\sin^2\theta}{2\sigma^2}\right)}{2\pi\sigma^2\left[1-\exp\left(\frac{-f^2\sin^2\theta_0}{2\sigma^2}\right)\right]} f^2\sin\theta\cos\theta d\theta d\varphi. \tag{26}$$

D. Force exerted by the entire beam

The force on the bead exerted by the entire beam can be written as

$$\vec{F} = \int_0^{2\pi}\int_0^{\theta_0} d\vec{F}. \tag{27}$$

As a consequence of the beam refraction at the glass-medium interface, θ_0 depends on the distance h from the center of the bead to the coverslip surface. Fewer rays reach the bead as h increases due to spherical aberration. If we set $h\sim a$, where a is the bead radius (so that the bead is nearly touching the coverslip), all rays that pass through the glass-water interface will reach the bead. Therefore, θ_0 is the critical angle for the glass-medium interface in this case. In typical experimental situations, the medium surrounding the beads is de-ionized water (n_m=1.343), so that θ_0=63.55°.

To carry out the integration in Eq. (27), we perform a change in variables. Observe that Q_t in Eq. (15) depends on the angles α and β. We write these angles as functions of θ and φ. We start with the aberration-free case and then include spherical aberration effects later.

1. Aberration-free case

Figure 6 shows a bead trapped by an optical tweezer. We represent the incident direction of a particular ray by the unit vector $\hat{z}'$ (cf. Fig. 4). Figure 6 depicts the general situation, where the sphere center is displaced by $\vec{r}$ from the objective focus (the origin of the reference frame). We denote by γ the angle between $\vec{r}$ and the z-axis. The vector $\vec{a}$ connects the center of the sphere to the point where the incident ray intersects the sphere, and $\vec{d}=\vec{r}+\vec{a}$.

From Fig. 6 we can write

$$\alpha = \arccos\left[\frac{d^2+a^2-r^2}{2ad}\right] \tag{28}$$

with

$$d = \sqrt{a^2-r^2+r^2(\sin\gamma\sin\theta\cos\varphi+\cos\gamma\cos\theta)^2} + r(\sin\gamma\sin\theta\cos\varphi+\cos\gamma\cos\theta). \tag{29}$$

The details are provided in Appendix A. The angle β is given by

$$n_m\sin\alpha = n_s\sin\beta, \tag{30}$$

where n_s is the sphere refractive index.

To complete the change in variables, we write the unit vectors $\hat{z}'$ and $\hat{y}'$ as functions of θ, φ, and the other parameters introduced in Fig. 6. The results are (see Appendix A)

$$\hat{z}' = (-\sin\theta\cos\varphi, -\sin\theta\sin\varphi, -\cos\theta) \tag{31}$$

and

$$\hat{y}' = \frac{\hat{z}'\times(\vec{r}\times\hat{z}')}{|\hat{z}'\times(\vec{r}\times\hat{z}')|}. \tag{32}$$

All the variables are now expressed in terms of the angles θ and φ, allowing the numerical calculation of the force using Eqs. (14) and (27).

2. Introducing spherical aberration

Figure 7 shows the general case, where the rays are refracted at the glass-water interface. Many experimental setups employ an oil immersion objective, with oil between the objective and the coverslip. There is no need to consider refraction at the oil-glass interface because the oil refractive index matches very closely the glass refractive index.[22,23] Nevertheless, it is important to consider refraction at the

glass-water interface, as indicated in Fig. 7. This refraction is related to spherical aberration, as discussed in Sec. I.

When we consider spherical aberration effects, each ray from the beam reaches the z-axis at a different point (see Fig. 7). Thus, there does not exist a single focal point but a focal region along the z-axis. To solve this problem, we consider a particular coordinate frame for each ray. We first write the force due to each ray relative to its particular coordinate frame, then we relate the variables in the particular coordinate frame to the variables in the principal coordinate frame. The origin of each particular coordinate frame is the point where the associated ray crosses the z-axis. The origin of the principal coordinate frame is the objective focus, the point to where all rays would converge in the aberration-free case, as depicted in Fig. 7.

In Fig. 7 $\vec{r}''$ and γ' are variables in the particular coordinate frame, and $\vec{r}$ and γ refer to the principal coordinate frames. The vector $\vec{a}''$ (with $|\vec{a}''|=a$) connects the center of the sphere to the point where the associated ray intersects the sphere, after refracting at the glass-water interface, and $\vec{d}''=\vec{r}''+\vec{a}''$. The vector $\vec{b}$ connects the origins of the two systems. The unit vectors $\hat{z}'$ and $\hat{z}''$ are along the incident direction of the ray before and after the refraction at the coverslip, respectively. The distance from the sphere center to the coverslip surface is represented by h, and L is the distance along the x-axis between the point where the particular ray reaches the coverslip and the z-axis. Finally, θ and ϕ are the incident and refraction angles at the glass-water interface, respectively.

For the particular coordinate frame, we can write

$$\alpha = \arccos\left[\frac{d''^2 + a^2 - r''^2}{2ad''}\right] \tag{33}$$

with

$$d'' = \sqrt{a^2 - r''^2 + r''^2(\sin\gamma''\sin\phi\cos\varphi + \cos\gamma''\cos\phi)^2} + r''(\sin\gamma''\sin\phi\cos\varphi + \cos\gamma''\cos\phi). \tag{34}$$

The parameters $\vec{r}''$ and γ' can be written as functions of the parameters related to the principal coordinate frame (see Appendix B) as

$$\cos\gamma'' = \frac{r\cos\gamma - b}{r''} \tag{35}$$

and

$$r'' = \sqrt{r^2 + b^2 - 2rb\cos\gamma} \tag{36}$$

with

$$b = \left(1 - \frac{n_m}{n_g}\frac{\cos\phi}{\cos\theta}\right)(h + r\cos\gamma). \tag{37}$$

The dependence on ϕ can be eliminated using

$$n_g \sin\theta = n_m \sin\phi. \tag{38}$$

To complete the solution, we write the unit vectors $\hat{z}''$ and $\hat{y}''$ as functions of the known parameters. Following Eqs. (31) and (32), we write

$$\hat{z}'' = (-\sin\phi\cos\varphi, -\sin\phi\sin\varphi, -\cos\phi) \tag{39}$$

and

$$\hat{y}'' = \frac{\hat{z}'' \times (\vec{r}'' \times \hat{z}'')}{|\hat{z}'' \times (\vec{r}'' \times \hat{z}'')|}. \tag{40}$$

Finally, the force exerted by a single ray on the bead can be written as

$$d\vec{F} = \frac{n_m}{c}T(\theta,\phi)[\mathrm{Re}(Q_t)\hat{z}'' + \mathrm{Im}(Q_t)\hat{y}'']dP. \tag{41}$$

Note that we have included the transmissivity $T(\theta,\phi)$ in Eq. (41) to account for the power loss when the beam passes through the coverslip.

By using Eq. (41), the force exerted by the entire beam can be calculated using Eq. (27). To numerically perform the integration, we write α and β as functions of ϕ using Eqs. (33), (34), and (30). Then, we write ϕ as a function of θ using Eq. (38) to obtain the total force in the geometrical optic approximation exerted by the optical tweezers on a microsphere, considering spherical aberration effects.

V. EXPERIMENTS

To calibrate the optical tweezers to perform quantitative measurements, we need to measure the trap stiffness κ. This parameter allows us to relate the position of the trapped bead in the potential well of the tweezers with the force exerted by the laser on the bead. For sufficiently small displacements, we have

$$F_x = -\kappa_x \Delta x, \tag{42}$$

where $\Delta x = x - x_0$ is the displacement from the equilibrium position x_0.

Similar expressions are valid for the other two directions, with stiffness κ_y and κ_z. Usually $\kappa_x = \kappa_y \gg \kappa_z$.[29,30] Some authors preferred to write $\kappa_x = \kappa_y$ as $\kappa_\parallel$ to emphasize that these two axes are parallel to the coverslip. The stiffness $\kappa_\parallel$ is relevant to bead movements parallel to the coverslip, and κ_z is relevant to bead movements perpendicular to the coverslip.

There are several experimental techniques to measure the trap stiffness of optical tweezers. The classic calibration uses a fluid chamber to compare the optical force with the force exerted by the fluid on the bead, which is given by Stokes' law,

$$F_s = 6\pi\eta a v, \tag{43}$$

where v is the bead velocity relative to the fluid in the chamber and η and a have their usual meanings. When the bead is near to a chamber wall, as in many experimental situations,[22,23] we should use Faxen's correction for Stokes' law,[32] which takes into account wall-drag effects.

If the bead is in an equilibrium position as the fluid flows, we can write $F_{\mathrm{optical}} = F_s$, which allows us to determine κ if we measure Δx and know η, a, and v. Ghislain *et al.*[33] and Simmons *et al.*[34] reported measurements using this idea.

Another kind of measurement consists of analyzing the backscattered light by the trapped bead.[35] Recently, Viana *et al.*[36] developed a light scattering technique to measure the trap stiffness of optical tweezers. This technique uses a second laser (He–Ne) collinear with the trapping laser (an infrared one) to study the intensity fluctuations of the backscattered light due to the bead's Brownian motion. Bead position fluctuations can be related to the fluctuations of the backscattered intensity, allowing the trap stiffness to be measured, because the bead position fluctuations increase as the stiff-

ness decreases.[36] This technique was used to measure the trap stiffness as a function of the bead radius for polystyrene and oil beads, and the results were compared to the Mie–Debye spherical aberration theory.[22,23] The details are described in Refs. 22, 23, and 36–39. In this paper, we use the experimental data reported in Refs. 22 and 23 to compare with the predictions of our geometrical optics model. Some alternative techniques for calibrating and measuring with optical tweezers can be found in Refs. 40–42.

VI. RESULTS AND DISCUSSION

The parameters employed in both numerical calculations and experiments are $\lambda=832$ nm, $P_l=4.8\pm0.2$ mW, $\sigma=1.2\pm0.1$ mm, NA=1.4, $n_s=1.496$ (oil beads), $n_m=1.343$ (de-ionized water), $h=a$, and $\theta_0=63.55°$. Spherical aberration effects are minimal when the bead is nearly touching the coverslip.

The parameters P_l, σ, n_s, n_m, h, and a were measured using experimental techniques described in Refs. 22, 23, and 36–39. The other parameters were given by the manufacturers.

A. Numerical results

1. Equilibrium position

To determine the trap stiffness κ, it is necessary to determine the equilibrium position $\vec{r}_{eq}$ of the bead in the potential well of the optical tweezers. In equilibrium the vector $\vec{r}$ (see Figs. 6 and 7) is parallel to the z-axis because the only effective force on the bead is exerted by the laser beam, which propagates in the z-direction before passing through the objective (see Fig. 5). The random forces exerted by the medium on the bead average to zero. Therefore, to find the equilibrium position $\vec{r}_{eq}$, it is sufficient that $F_z=0$, where F_z is the trapping force along the z direction.

To perform the numerical calculations, we use Eq. (27) to determine the force and its components. The condition $F_z=0$ can be used to determine $\vec{r}_{eq}$ (and the angle γ).

The numerical results show that $\vec{r}_{eq}/a$ is constant for any a value; that is, the equilibrium position is proportional to the bead radius in the geometrical optics regime. In the aberration-free case, we find $r_{eq}/a=0.239$ and $\gamma=\pi$, which means that the sphere center stays above the objective focus in this situation. If there is aberration, we find $r_{eq}/a=0.032$ and $\gamma=0$; that is, the sphere center stays below the objective focus. The calculations were repeated for several values of a to verify that $\vec{r}_{eq}/a$ is constant. These results show that the bead stays trapped by the laser beam in the equilibrium position $\vec{r}_{eq}$.

2. Trapping force along the x direction

To evaluate the trapping force along the x direction, we displace the bead by Δx from its original equilibrium position $\vec{r}_{eq}$. This displacement can be performed numerically by adding a component to $\vec{r}_{eq}$ along the x direction: $\vec{r}=\vec{r}_{eq}+\Delta x\hat{x}$ (see Fig. 8).

The numerical results show that the force F_x points in the opposite direction of the vector $\Delta x\hat{x}$. Hence, the calculated equilibrium positions $\vec{r}_{eq}$ are stable and characterize a potential well generated by the optical tweezers. We find that F_x is proportional to the displacement Δx, that is, κ_x is a constant. We conclude that the bead trapped by the optical tweezers is similar to a harmonic oscillator, with a constant stiffness for small displacements Δx. Figure 9 shows the force F_x as a function of Δx for an oil bead with $a=1.0$ μm, including spherical aberration.

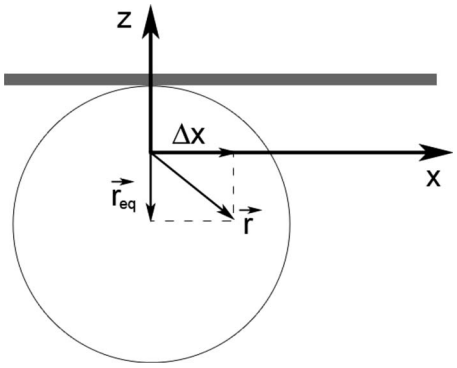

Fig. 8. Schematic of the method used to calculate F_x.

3. Trap stiffness: Comparison with experimental data

To compare the calculated geometrical optics model with experimental data, we plot κ_x/P_l as a function of the bead radius because κ_x is proportional to the value of P_l (the tweezers become stiffer if the laser power is increased).[22,23] Figure 10 shows the numerical results obtained with the geometrical optics model for $a>\lambda$. We also include experimental data from Refs. 22 and 23 to compare with the numerical results.

Observe that the geometrical optics calculations including spherical aberration lead to lower stiffness values for each bead radius compared to the aberration-free situation. This result was expected because spherical aberration decreases the trap efficiency, as discussed. Figure 10 shows that the two curves are very close, indicating that spherical aberration does not appreciably change the results in the geometrical optics regime. This fact also occurs for other kinds of microspheres, such as those made of polystyrene,[22,23] because the aberration is minimal for $h\sim a$, as expected. In addition, the aberration is weaker for larger beads, such as those employed in the geometrical optics regime.

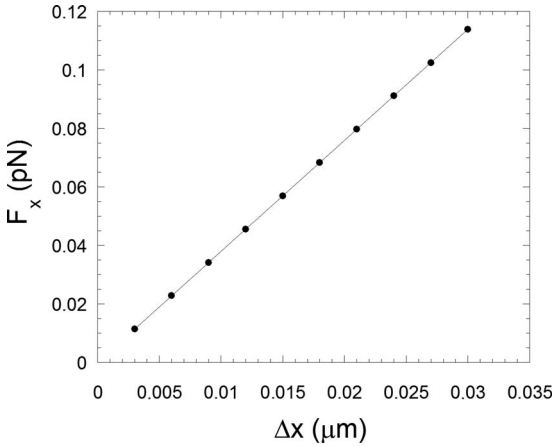

Fig. 9. Plot of the force versus the displacement along the x direction for an oil bead with $a=1.0$ μm, considering spherical aberration. The graph is linear, which means that the trap stiffness κ_x is constant.

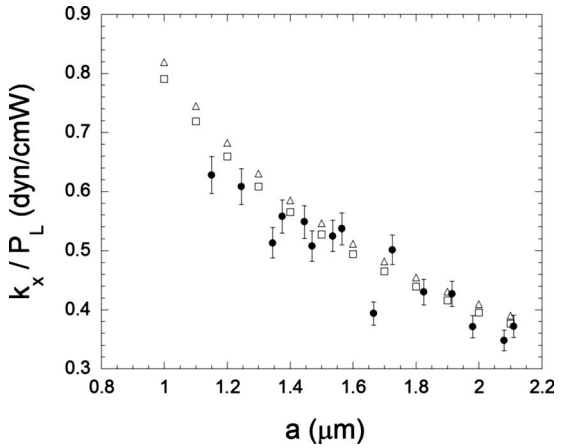

Fig. 10. Transverse trap stiffness divided by the local power as a function of bead radius: experimental data (circles), geometrical optics model considering spherical aberration (squares), and geometrical optics aberration-free model (triangles).

Note that the theoretical curves shown in Fig. 10 are hyperbolas; that is, the trap stiffness is proportional to $1/a$ in the geometrical optics regime. This relation means that geometrical optics predicts an infinite trap stiffness as $a \to 0$, which does not correspond to reality. For $a \ll \lambda$, the geometrical optics treatment fails and we must use the Rayleigh treatment (see Sec. III) or the Mie–Debye spherical aberration theory, which is valid for beads of all sizes.[22,23]

B. Experimental results

We used the light scattering method[22,23,36] and the parameters described in Sec. V to determine the tweezers' trap stiffness κ_x using oil beads in water. The results for $a > \lambda$ are displayed in Fig. 10. Each point shown in Fig. 10 was determined by performing an average over results from ten different beads of the same radius. The error bars were determined by calculating the standard error from the mean value for each point. The agreement between the experimental and the geometrical optics calculations is quite good in this region even for $a \gtrsim \lambda$. Similar agreement was found for polystyrene beads in water,[23] showing that the geometrical optics model works well. The agreement is better as the radius a increases (for fixed λ). We conclude that the procedure for calculating the trap stiffness is reliable in the geometrical optics regime and can be easily implemented even when incorporating spherical aberration. Note that all the parameters used in the theoretical calculations were measured and that there are no adjustable parameters.

VII. MIE–DEBYE SPHERICAL ABERRATION THEORY OF OPTICAL TWEEZERS

Even though optical tweezers have been extensively used for more than 20 years, an exact theoretical treatment has been developed only recently.[29,30] This treatment is based on a realistic, Debye-type representation for the strongly focused laser beam beyond the microscope objective,[43] and on Mie scattering theory for the beam interaction with the microsphere, also including spherical aberration effects. The treatment is known as the Mie–Debye spherical aberration theory of optical tweezers and consistently covers all regimes from the Rayleigh limit up to the geometrical optics limit. An important feature of the Mie–Debye spherical aberration theory is that it is formulated entirely in terms of the experimentally accessible data, with no adjustable parameters. The parameters that must be measured to calculate the trap stiffness are the power and profile of the laser beam at the objective entrance, the numerical aperture and transmittance of the objective, the refractive indices of the bead and medium, and the bead radius. In Ref. 23 we discuss some techniques to measure these parameters.

In Refs. 22 and 23 we compared the predictions of the Mie–Debye spherical aberration theory and measurements for oil and polystyrene beads, covering all regimes of bead sizes. We found good agreement between theory and experiment, showing that absolute calibration of optical tweezers is possible, which is very useful to experimentalists.

ACKNOWLEDGMENTS

The author thanks N. B. Viana, O. N. Mesquita, A. Mazolli, P. A. M. Neto, and H. M. Nussenzveig for all the helpful discussions during the past several years.

APPENDIX A: CHANGE IN VARIABLES IN THE ABERRATION-FREE CASE

All calculations in this appendix are based on Fig. 6. We write $\vec{d}$ in spherical coordinates as

$$\vec{d} = (d \sin\theta \cos\varphi, d \sin\theta \sin\varphi, d \cos\theta). \tag{A1}$$

We choose the plane $y=0$ to go through the center of the sphere and write

$$\vec{r} = (r \sin\gamma, 0, r \cos\gamma). \tag{A2}$$

To express $\vec{d}$ as a function of r, γ, θ, and φ, we note that

$$|\vec{d} - \vec{r}| = a, \tag{A3}$$

which gives

$$d^2 + r^2 - 2rd(\sin\gamma \sin\theta \cos\varphi + \cos\gamma \cos\theta) = a^2. \tag{A4}$$

The solution of Eq. (A4) for d gives Eq. (29). By using the triangle formed by $\vec{d}$, $\vec{r}$, and $\vec{a}$, we get

$$r^2 = d^2 + a^2 - 2ad \cos\alpha, \tag{A5}$$

which leads to Eq. (28). To obtain the unit vectors $\hat{z}'$ and $\hat{y}'$, we observe that $\hat{z}'$ is antiparallel to $\vec{d}$. We obtain Eq. (31) with the help of Eq. (A1). We use the fact that the unit vector $\hat{y}'$ is parallel to the vector $\hat{z}' \times (\vec{r} \times \hat{z}')$ to derive Eq. (32).

APPENDIX B: CHANGE IN VARIABLES CONSIDERING SPHERICAL ABERRATION

All calculations in this appendix are based on Fig. 7. Equations (33) and (34) are obtained by the same procedure employed in the aberration-free case. The vectors $\vec{r}$ and $\vec{r}''$ are related by

$$\vec{r} - \vec{b} = \vec{r}'', \tag{B1}$$

which gives

$$r'' = \sqrt{r^2 + b^2 - 2rb\cos\gamma}. \tag{B2}$$

The angle γ'' can be obtained by taking the scalar product of Eq. (B1) with $\vec{b}$,

$$r''b\cos\gamma'' = rb\cos\gamma - b^2, \tag{B3}$$

which leads directly to Eq. (35).

We write $\vec{b}$ as a function of the known parameters by observing that we can write (see Fig. 7)

$$\tan\phi = \frac{L}{h - b - r\cos(\pi - \gamma)} \tag{B4}$$

and

$$\tan\theta = \frac{L}{h - r\cos(\pi - \gamma)}. \tag{B5}$$

Equations (B4) and (B5), and Eq. (38) can be manipulated to derive Eq. (37).

[a]Electronic mail: marcios.rocha@ufv.br

[1] A. Ashkin, "Acceleration and trapping of particles by radiation pressure," Phys. Rev. Lett. **24**(4), 156–159 (1970).

[2] A. Ashkin, "Forces of a single-beam gradient laser trap on a dielectric sphere in the ray optics regime," Biophys. J. **61**(2), 569–582 (1992).

[3] A. Ashkin, "Optical trapping and manipulation of neutral particles using lasers," Proc. Natl. Acad. Sci. U.S.A. **94**(10), 4853–4860 (1997).

[4] A. Ashkin and J. M. Dziedzic, "Optical trapping and manipulation of viruses and bacteria," Science **235**(4795), 1517–1520 (1987).

[5] K. Svoboda and S. M. Block, "Biological applications of optical forces," Annu. Rev. Biophys. Biomol. Struct. **23**, 247–285 (1994).

[6] D. G. Grier, "A revolution in optical manipulation," Nature (London) **424**(6950), 810–816 (2003).

[7] M. J. McCauley and M. C. Williams, "Mechanisms of DNA binding determined in optical tweezers experiments," Biopolymers **85**(2), 154–168 (2007).

[8] M. S. Rocha, N. B. Viana, and O. N. Mesquita, "DNA-psoralen interaction: A single molecule experiment," J. Chem. Phys. **121**(19), 9679–9683 (2004).

[9] M. S. Rocha, M. C. Ferreira, and O. N. Mesquita, "Transition on the entropic elasticity of DNA induced by intercalating molecules," J. Chem. Phys. **127**(10), 105108-1–7 (2007).

[10] M. D. Wang, H. Yin, R. Landick, J. Gelles, and S. M. Block, "Stretching DNA with optical tweezers," Biophys. J. **72**(3), 1335–1346 (1997).

[11] I. D. Vladescu, M. J. McCauley, I. Rouzina, and M. C. Williams, "Mapping the phase diagram of single DNA molecule force-induced melting in the presence of ethidium," Phys. Rev. Lett. **95**, 158102-1–4 (2005).

[12] J. Liphardt, B. Onoa, S. B. Smith, I. Tinoco, Jr., and C. Bustamante, "Reversible unfolding of single RNA molecules by mechanical force," Science **292**(5517), 733–737 (2001).

[13] C. Bustamante, J. Liphardt, and F. Ritort, "The nonequilibrium thermodynamics of small systems," Phys. Today **58**(7), 43–48 (2005).

[14] J. Dharmadhikari, S. Roy, A. Dharmadhikari, S. Sharma, and D. Mathur, "Torque-generating malaria-infected red blood cells in an optical trap," Opt. Express **12**(6), 1179–1184 (2004).

[15] S. Mohanty, K. Mohanty, and P. Gupta, "Dynamics of Interaction of RBC with optical tweezers," Opt. Express **13**(12), 4745–4751 (2005).

[16] A. S. Khalil, J. M. Ferrer, R. R. Brau, S. T. Kottmann, C. J. Noren, M. J. Lang, and A. M. Belcher, "Single M13 bacteriophage tethering and stretching," Proc. Natl. Acad. Sci. U.S.A. **104**(12), 4892–4897 (2007).

[17] K. C. Neuman and S. M. Block, "Optical trapping," Rev. Sci. Instrum. **75**(9), 2787–2809 (2004).

[18] J. R. Moffitt, Y. R. Chemla, S. B. Smith, and C. Bustamante, "Recent advances in optical tweezers," Annu. Rev. Biochem. **77**, 205–228 (2008).

[19] A. Rohrbach and E. H. K. Stelzer, "Trapping forces, force constants, and potential depths for dielectric spheres in the presence of spherical aberrations," Appl. Opt. **41**(13), 2494–2507 (2002).

[20] A. Rohrbach, "Stiffness of optical traps: Quantitative agreement between experiment and electromagnetic theory," Phys. Rev. Lett. **95**(16), 168102-1–4 (2005).

[21] G. Roosen, "La lévitation optique de sphères," Can. J. Phys. **57**(9), 1260–1279 (1979).

[22] N. B. Viana, M. S. Rocha, O. N. Mesquita, A. Mazolli, P. A. Maia Neto, and H. M. Nussenzveig, "Absolute calibration of optical tweezers," Appl. Phys. Lett. **88**(13), 131110-1–3 (2006).

[23] N. B. Viana, M. S. Rocha, O. N. Mesquita, A. Mazolli, P. A. Maia Neto, and H. M. Nussenzveig, "Towards absolute calibration of optical tweezers," Phys. Rev. E **75**(2), 021914-1–13 (2007).

[24] H. Felgner, O. Muller, and M. Schliwa, "Calibration of light forces in optical tweezers," Appl. Opt. **34**(6), 977–982 (1995).

[25] P. C. Ke and M. Gu, "Characterization of trapping force in the presence of spherical aberration," J. Mod. Opt. **45**(10), 2159–2168 (1998).

[26] E. Fallman and O. Axner, "Influence of a glass-water interface on the on-axis trapping of micrometer-sized spherical objects by optical tweezers," Appl. Opt. **42**(19), 3915–3926 (2003).

[27] E. Theofanidou, L. Wilson, W. J. Hossack, and J. Arlt, "Spherical aberration correction for optical tweezers," Opt. Commun. **236**(1-3), 145–150 (2004).

[28] K. C. Vermeulen, G. J. L. Wuite, G. J. M. Stienen, and C. F. Schmidt, "Optical trap stiffness in the presence and absence of spherical aberrations," Appl. Opt. **45**(8), 1812–1819 (2006).

[29] P. A. Maia Neto and H. M. Nussenzveig, "Theory of optical tweezers," Europhys. Lett. **50**(5), 702–708 (2000).

[30] A. Mazolli, P. A. Maia Neto, and H. M. Nussenzveig, "Theory of trapping forces in optical tweezers," Proc. R. Soc. London, Ser. A **459**(2040), 3021–3041 (2003).

[31] J. D. Jackson, *Classical Electrodynamics*, 3rd ed. (Wiley, New York, 1998).

[32] H. Faxen, "The resistance against the movement of a rigour sphere in viscous fluids, which is embedded between two parallel layered barriers," Ann. Phys. **68**(10), 89–119 (1922).

[33] L. P. Ghislain, N. A. Switz, and W. W. Webb, "Measurement of small forces using an optical trap," Rev. Sci. Instrum. **65**, 2762–2768 (1994).

[34] R. M. Simmons, J. T. Finer, S. Chu, and J. A. Spudich, "Quantitative measurements of force and displacement using an optical trap," Biophys. J. **70**(4), 1813–1822 (1996).

[35] M. E. J. Friese, H. Rubinsztein-Dunlop, N. R. Heckenberg, and E. W. Dearden, "Determination of the force constant of a single-beam gradient trap by measurement of backscattered light," Appl. Opt. **35**(36), 7112–7116 (1996).

[36] N. B. Viana, R. T. S. Freire, and O. N. Mesquita, "Dynamic light scattering from an optically trapped microsphere," Phys. Rev. E **65**(4), 041921-1–11 (2002).

[37] N. B. Viana, O. N. Mesquita, and A. Mazolli, "In situ measurement of laser power at the focus of a high numerical aperture objective using a microbolometer," Appl. Phys. Lett. **81**(10), 1765–1767 (2002).

[38] N. B. Viana, M. S. Rocha, and O. N. Mesquita, "In situ laser power measurement at the focus of microscope objectives used in optical tweezers," Am. J. Phys. **73**(3), 201–205 (2005).

[39] N. B. Viana, M. S. Rocha, O. N. Mesquita, A. Mazolli, and P. A. Maia Neto, "Characterization of objective transmittance for optical tweezers," Appl. Opt. **45**(18), 4263–4269 (2006).

[40] S. F. Tolić-Nørrelykke, E. Schafferb, J. Howard, F. S. Pavone, F. Julicher, and H. Flyvbjerg, "Calibration of optical tweezers with positional detection in the back focal plane," Rev. Sci. Instrum. **77**(10), 103101-1–11 (2006).

[41] K. Berg-Sørensen, L. Oddershede, Ernst-Ludwig Florin, and H. Flyvbjerg, "Unintended filtering in a typical photodiode detection system for optical tweezers," J. Appl. Phys. **93**, 3167–3176 (2003).

[42] D. C. Appleyard, K. Y. Vandermeulen, H. Lee, and M. J. Lang, "Optical trapping for undergraduates," Am. J. Phys. **75**(1), 5–14 (2007).

[43] B. Richards and E. Wolf, "Electromagnetic diffraction in optical systems. 2. Structure of the image field in an aplanatic system," Proc. R. Soc. London, Ser. A **253**(1274), 358–379 (1959).